Mechanical Systems and Signal Processing 203 (2023) 110713

Contents lists available at ScienceDirect

Mechanical Systems and Signal Processing

journal homepage: www.elsevier.com/locate/ymssp

Particle filter-based damage prognosis using online feature fusion and selection

Tianzhi Li [a], Jian Chen [b], Shenfang Yuan [b], Francesco Cadini [a], Claudio Sbarufatti [a,*]

[a] Dipartimento di Meccanica, Politecnico di Milano, Milan, Italy
[b] Research Center of Structural Health Monitoring and Prognosis, State Key Laboratory of Mechanics and Control of Mechanical Structures, Nanjing University of Aeronautics and Astronautics, Nanjing, China

ARTICLE INFO

Communicated by Xiaosheng Si

Keywords:
Structural health monitoring
Damage prognosis
Feature fusion and selection
Particle filter
Lamb wave

ABSTRACT

Damage prognosis generally resorts to damage quantification functions and evolution models to quantify the current damage state and to predict the future states and the remaining useful life (RUL). The former typically consists of a function describing the relationship between the damage state and a statistical feature extracted from the measured signals, thus the prognostic performance will strongly depend on the selection of a proper feature. Given the best feature may vary for different specimens or even at each time instant for the same specimen during damage progression, such selection is a challenging task but has received little investigation so far. In this context, this paper proposes a particle filter-based damage prognosis framework, which involves an online feature fusion and selection scheme. A prognostic model is considered for each feature, with a multivariate process equation, formulated using both a damage degradation function and a bias parameter, and a measurement equation linking the damage state and that feature considering a data-driven model and the bias. One PF is used to estimate the damage state, its evolution parameters, and the bias for each model. Then, at each step, the feature with the smallest estimated bias is selected as the best feature providing the most likely state vectors and is used to select the most likely samples of the damage state and growth parameters for predicting the RUL and for calculating the prior at the next step. The proposed prognostic framework is demonstrated by an experimental study, where an aluminum lug structure subject to fatigue crack growth is monitored by a Lamb wave measurement system.

1. Introduction

Degradation is an inevitable phenomenon in structures, where damage can evolve over time or with the number of load cycles. Eventually, safety may no longer be guaranteed when the damage state reaches a predefined threshold. Regular inspections should be carried out to evaluate functionality but they require high financial expenses and unwanted system shutdowns. One possibility for simultaneously ensuring structural safety and reducing maintenance costs is to schedule maintenance just before the damage state reaches the critical limit. In this context, the structure's remaining useful life (RUL), i.e., the time required by the component or structure to reach its operative limit, is desired to be estimated online by an advanced damage prognosis technique.

Structural degradation can be defined through either (i) a physics-based damage state, e.g. including matrix crack density [1],

* Corresponding author.
E-mail address: claudio.sbarufatti@polimi.it (C. Sbarufatti).

https://doi.org/10.1016/j.ymssp.2023.110713
Received 16 April 2023; Received in revised form 4 July 2023; Accepted 21 August 2023
Available online 4 September 2023

delamination length [2], delamination shape [3], or stiffness reduction [4,5] for composites, and crack length [6–9] or shape [10] in metals, or (ii) some sort of data-driven health indicators [11–13] extracted from online measurements like acoustic emission and strain. Provided that degradation can follow a certain pattern under a specific input load condition, the future damage condition can be projected by the current state through a model. Depending on the type of information used for degradation modeling, namely physical knowledge or experimental and in-field data, damage evolution models can be classified either as physics-based [1,2,6–10] or data-driven [3,5,11,14]. The former generally falls into the scope of Paris' law or its extensions, where the rate of damage evolution, e.g., strain energy release rate or stress intensity factor, is either analytically calculated [1,2,8] or fitted from numerical simulations through a data-driven modeling strategy such as polynomial fitting [6,7], support vector regression [10], or neural networks [9]. On the other hand, pure data-driven approaches, including polynomial fitting [3], neural networks [5,14], or Markov models [11], are usually built through sufficient damage data or health indicators measured during the experimental or in-field degradation process.

However, given the uncertainties related to complex structural degradations [15], environmental effects [16], and sensor health conditions [16], a deterministic damage evolution model itself can hardly yield an accurate prognostic result, even in different replicas of the same structure or specimen. One possibility is to set some model parameters as unknown variables to be online updated by a state estimation technique, such as particle filter (PF), widely implemented for non-linear and non-Gaussian problems [17,18]. This, on the other hand, implies a direct or indirect damage quantification scheme. The former implies the direct measure of a damage state, e.g., measuring the matrix crack density and delamination area through X-ray [1,19], or extracting some residual strength indicators from the online measured signals [20–22]. The latter resorts to online measurement which must then be correlated to damage states through a measurement equation. Typical examples includes sensor networks based on fiber Bragg grating strain sensors [2,23], Lamb wave-based monitoring systems [6,24,25], or accelerometers [26,27]. Such measurement equation, linking the damage state with some damage-sensitive features obtained from measurements, can be physical or, in most cases, it is fitted by a data-driven technique, e.g., neural network [2,23], polynomial function [6], leave-one-out method [24] or Gaussian process regression [28]. However, the implementation of this measurement equation poses some challenges.

First, the relationship between the damage state and the observed feature(s) can vary in different replicas of the same structure due to the uncertainties mentioned above, inevitably inducing a bias between the observed features and those predicted by the measurement equation, eventually deteriorating the prognostic performance if not properly considered [3,6]. Few prognostic studies [3,6,29] aimed to alleviate the effect of such bias, where one or more bias parameters are included in the measurement equation and are online estimated for error compensation.

Second, one feature is typically used for building the measurement equation in [3,6,29]. When more features are embedded into the measurement equation, each one potentially affected by a bias, multiple bias parameters should be included in the state space for identification and error compensation, possibly suffering from the curse of dimensionality, and eventually leading to an inaccurate state and parameter estimation. As a result, the prognostic performance will strictly depend on the selection of a proper feature, which is not a trivial task, especially considering the best feature may vary in different replicas of the same structure, or even, at different time instants during damage progression on the same structure or specimen. This naturally calls for an integrated framework to fuse multiple features (feature fusion) and to online select the best ones (feature selection) for identifying the current damage state, which, however, has received little attention in current prognostic practices.

Feature fusion and selection have been investigated in some pure data-driven RUL prediction studies [12,22], where three main steps are typically included, i.e., (i) extracting some statistical features from the measured signals, then (ii) fusing multiple features or selecting the best ones through a proposed metric or criterion for building the health indicator (HI), finally (iii) calculating the RUL through a model describing the relationship between the RUL and the HI. As the sensitivity of each feature to the HI construction can vary during the whole run-to-failure process, an online feature fusion and selection scheme is always desired but has received very few investigation [21], where each feature is weighted at each time step for building a proper HI. On the other hand, feature fusion and selection have also been applied to damage quantification in [30,31], where an offline selection scheme has been adopted. In conclusion, limited attention has been given to online feature fusion and selection. Furthermore, the strategies for effectively mitigating the bias associated with each feature have yet to be thoroughly explored.

In this context, combining the bias-based prognostic model proposed by the authors in [6] with the general idea of feature selection, this paper develops a PF-based prognostic framework, where the bias of each feature used is online estimated by PF, and an online feature fusion and selection scheme is proposed based on the estimated bias. More specifically, each bias-based prognostic model is built by a different feature, and then processed through one particle filter (PF), thus the bias between the predicted and observed feature can be online taken into account. Moreover, a general principle arising from [6] is that, among multiple features applied to the same specimen, the feature associated with a lower bias level tends to offer superior prognostic performance. Thus the feature (or group of particles) exhibiting the smallest estimated bias is chosen as the best for that specific step. Given that the best feature can vary at different steps, the fusion process is achieved by utilizing the particles from different best features at different steps throughout the entire run-to-failure process. The proposed prognostic framework is demonstrated by an experimental study, where an aluminum lug structure subject to fatigue crack growth (FCG) is monitored by a Lamb wave measurement system.

The rest of this paper is organized as follows: Section 2 defines the novel prognostic framework. The application setup is shown in Section 3, while the results of the proposed method for the experimental case study are provided in Section 4. Finally, Section 5 concludes this paper.

2. Novel damage prognosis framework

Fig. 1 presents the four main steps of the proposed damage prognosis framework, namely, (i) formulate some independent

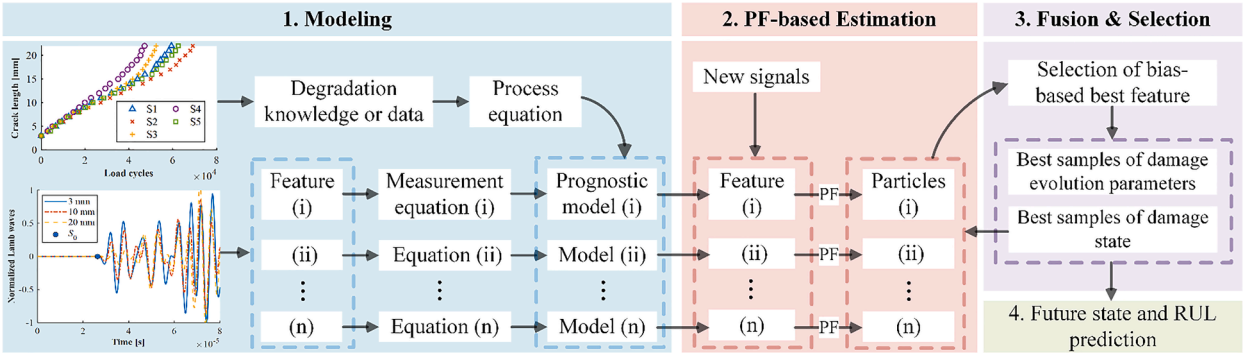

Fig. 1. Novel particle filter (PF)-based damage prognosis framework with embedded feature fusion and selection.

prognostic models, each with one associated observed feature [6,7], (ii) estimate the damage state, the damage evolution model parameters, and the bias for each prognostic model by one PF, (iii) select the feature with the smallest estimated bias as the best and substitute its damage state samples into those samples from the other features, and (iv) project damage state into the future by the process equation starting from the damage state samples associated with the best feature. Compared to the traditional method [6,7], where PF is only applied to one prognostic model to provide the samples for predicting the future state and RUL, the main novelty of the proposed method is that a fusion and selection scheme is online implemented to identify the best feature at each step, then adopting its samples for the health state and RUL calculations.

2.1. Bias-based prognostic model

The damage evolution with time or the number of load cycles is usually discretized as

$$x_k = f(x_{k-1}, \theta) \tag{1}$$

where x is the damage state, $f(\bullet)$ is the evolution function that is derived from either physical knowledge or damage data, $\boldsymbol{\theta}$ is a vector of damage evolution parameters, and the subscript k denotes the k-th time step. Then, the parameters $\boldsymbol{\theta}$ are usually treated as some unknown variables in the state vector to be updated [6,24],

$$\begin{bmatrix} \theta_k \\ x_k \end{bmatrix} = \begin{bmatrix} \theta_{k-1} + \boldsymbol{\omega}_{\theta,k} \\ f(x_{k-1}, \theta_k, \omega_k) \end{bmatrix} \tag{2}$$

where ω_k and $\boldsymbol{\omega}_\theta$ are the process noises for the damage state and model parameters, respectively.

When some indirect online measurement systems like Lamb wave are applied, some sort of statistical feature is usually extracted from the measured signals for damage quantification. With a proper measurement y_l (i.e., the l-th feature extracted from those signals) for inferring the unknown damage state, the measurement equation in a PF-based damage prognosis can be formulated as:

$$y_{l,k} = g_l(x_k) + \nu_k \tag{3}$$

where $g_l(\bullet)$ is usually a data-driven function describing the relationship between the damage state and the l-th feature, ν_k is the measurement noise. To cope with the unavoidable bias between the observed and predicted measurements, the bias-based prognostic model taken from the work of the same authors [3,6] is adopted here to guarantee sufficient estimation accuracy. For the l-th feature, its model can be formulated as:

$$\begin{cases} \boldsymbol{z}_{l,k} = \begin{bmatrix} \theta_k \\ x_k \\ b_{l,k} \end{bmatrix} = \begin{bmatrix} \theta_{k-1} + \boldsymbol{\omega}_{\theta,k} \\ f(x_{k-1}, \theta_k, \omega_k) \\ b_{l,k-1} + \omega_{l,b,k} \end{bmatrix} \\ y_{l,k} = g_l(x_k) + b_{l,k} + \nu_{l,k} \end{cases} \tag{4}$$

where b is the bias parameter, variable with time, ω_b is its corresponding process noise, and z_k is a newly defined augmented state vector. Note the number of models built in this study is equal to the number (L) of available features $l = 1, \cdots, L$. Additionally, to facilitate an accurate comparison between the performance of multiple prognostic models and that of a single model, this study incorporates a shared damage evolution model among each prognostic model. While it is not mandatory to use the same damage evolution model across different prognostic models in this application, it is generally permissible to employ different damage evolution models if desired or applicable.

Table 1
Sampling importance resampling particle filter.

Initialization: draw N_p particles $\left\{z_{l,0}^i : i = 1, 2, \cdots, N_p\right\}$ from the initial distribution $p(z_{l,0})$
For $k = 1, 2, \ldots,$
- **Prediction** in PF: draw N_p particles $\left\{z_{l,k}^i : i = 1, 2, \cdots, N_p\right\}$ by $z_{l,k}^i\ p(z_{l,k}|z_{l,k-1}^i)$
- **Weight update**: calculate the weight w_k^i by $w_k^i \propto p(y_{l,k}|z_{l,k}^i)$, and assign its normalized form $\tilde{w}_k^i$ to each particle $z_{l,k}^i$
- **Resample** for $\left\{z_{l,k}^i : i = 1, 2, \cdots, N_p\right\}$ using the particle weights $\left\{\tilde{w}_k^i : i = 1, 2, \cdots, N_p\right\}$

End

Table 2
Proposed feature fusion and selection scheme.

Provided with resampled particles at k-th step from each PF
For $l = 1, 2, \cdots, L$
- **Select** the bias samples $\left\{b_{l,k}^i : i = 1, 2, \cdots, N_p\right\}$ from the particles $\left\{z_{l,k}^i : i = 1, 2, \cdots, N_p\right\}$
- **Calculate** the root-mean-square (RMS) value of the bias samples

End
Define the feature with the smallest bias RMS value as the best, and its particles as $\left\{z_{best,k}^i : i = 1, 2, \cdots, N_p\right\}$
For $l = 1, 2, \cdots, L$
- **Replace** the damage state samples within $\left\{z_{l,k}^i : i = 1, 2, \cdots, N_p\right\}$ by those within $\left\{z_{best,k}^i : i = 1, 2, \cdots, N_p\right\}$

End

2.2. Particle filter-based estimation

When a Bayesian approach is applied to the l-th prognostic model, the unknown state vector $z_{l,k}$ can be inferred from the measurement as:

$$p(z_{l,k}|\boldsymbol{y}_{l,1:k-1}) = \int p(z_{l,k}|z_{l,k-1}) p(z_{l,k-1}|\boldsymbol{y}_{l,1:k-1}) dz_{l,k-1} \tag{5}$$

$$p(z_{l,k}|\boldsymbol{y}_{l,1:k}) \propto p(y_{l,k}|z_{l,k}) p(z_{l,k}|\boldsymbol{y}_{l,1:k-1}) \tag{6}$$

where $\boldsymbol{y}_{l,1:k}$ is the measurement vector collected from time step 1 to k, the symbol $\propto$ indicates proportionality, the transition distribution $p(z_{l,k}|z_{l,k-1})$ and the likelihood function $p\left(y_{l,k}|z_{l,k}\right)$ denote the process and measurement equations, respectively, $p\left(z_{l,k}|\boldsymbol{y}_{l,1:k-1}\right)$ and $p\left(z_{l,k}|\boldsymbol{y}_{l,1:k}\right)$ are the prior and posterior-updated probability distribution function (PDF) of the augmented state vector, respectively.

Eqs. (5) and (6) form the basis of the optimal Bayesian solution, which is, however, difficult to be analytically calculated in a nonlinear and non-Gaussian system like Eq. (4). Therefore, an efficient state estimation algorithm, i.e., the sampling importance resampling (SIR) PF [32], is used in this study. Table 1 lists the pseudo-code of the SIR PF.

2.3. Online fusion and selection

Consider that there are multiple bias-based prognostic models, each based on a different feature and then independently applied to the same specimen through one PF. As a smaller bias between the predicted and observed feature induces a minor effect on the damage state quantification, the feature (or group of particles) having the smallest bias at one step is deemed the best at that step. This, as a consequence, leads to the strategy of online defining the best feature based on bias. Moreover, provided that all groups of particles share a damage state variable, one possibility for enhancing the prognostic performance is to substitute the damage state samples obtained by the best feature (or group of particles) into those samples from the other features (or groups of particles) for the one-step-ahead prior calculation.

As, in real applications, the direct measurement of damage is not always available, thus impeding the calculation of the true bias, one alternative is to approximate the bias by PF and subsequently use that for selecting the best feature. The online fusion and selection procedure is implemented at each time step as follows,

(i) calculating the root-mean-square (RMS) value of bias samples from each feature (or group of particles),
(ii) defining the feature (or group of particles) with the smallest RMS as the best feature (or group of particles) for that step,
(iii) adopting the samples of crack length and growth parameters (x and $\boldsymbol{\theta}$) from the best feature for calculating the future state and RUL, and the crack length samples (x) to replace those samples associated with the other less performing features.

Table 3
Calculation of future state and RUL at time step k.

Initialization: define samples of the damage state and evolution parameters from $\left\{z^i_{best,k} : i = 1, 2, \cdots, N_p\right\}$ as $\left\{x^{i,0}_k : i = 1, 2, \cdots, N_p\right\}$ and $\left\{\theta^i_{best,k} : i = 1, 2, \cdots, N_p\right\}$, respectively
For $i = 1{:}N_p$
  $j = 0$
  While $x^{i,j}_k < l_{th}$
    Calculate the future state $x^{i,j+1}_k$ by $x^{i,j+1}_k = f\left(x^{i,j}_k, \theta^i_{best,k}\right)$
    $j = j + 1$
  End
  $\mathrm{RUL}^i_k = j \times \Delta N$
End

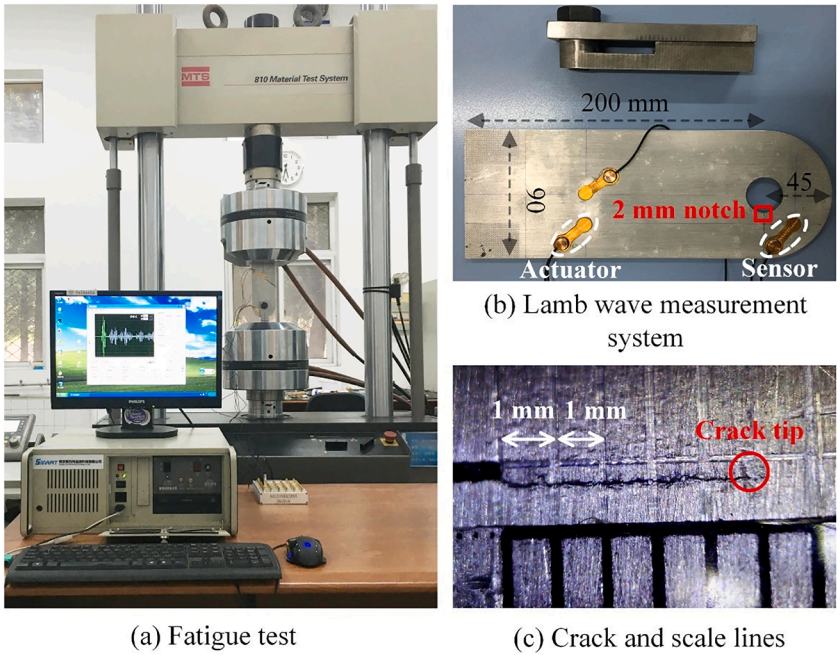

(a) Fatigue test
(b) Lamb wave measurement system
(c) Crack and scale lines

Fig. 2. Experimental setup.

Since the best feature can differ at different steps, the fusion is automatically accomplished by incorporating the samples from different features during the whole estimation process. Note that the $\boldsymbol{\theta}$ -samples from the best feature are not involved in such substitution. We assume the bias only has a direct relationship with the damage state arising from the measurement equation, and not with parameters governing the damage growth process. Moreover, this provides room for future development regarding the utilization of different damage evolution models. Table 2 lists the pseudo-code of the above procedure.

2.4. Calculation of future state and RUL

Within a PF-based prognostic framework, the prognostic step enables the prediction of future damage states through the degradation model Eq. (1) and based on the particles filtered by the best feature. The prediction for each particle stops when the future state reaches a pre-defined threshold value of the damage state l_{th}. Then, the RUL is deemed to be equal to the multiplication of the number of prediction steps by the number of load cycles ΔN in one step. The procedure is outlined by the pseudo-code in Table 3.

3. Application setup

This section introduces the experimental and numerical application setups. More specifically, the fatigue tests of five aluminum lug structures and the Lamb wave monitoring system are briefly introduced in Section 3.1; Section 3.2 presents the numerical simulations of the Lamb waves at different crack lengths [7]; the Lamb waves from both the experimental and numerical studies are processed to provide four different statistical features for damage quantification in Section 3.3; Section 3.4 presents the formulation of Paris' law-based process equation and feature-based measurement equation, and the PF hyperparameters applied to each prognostic model;

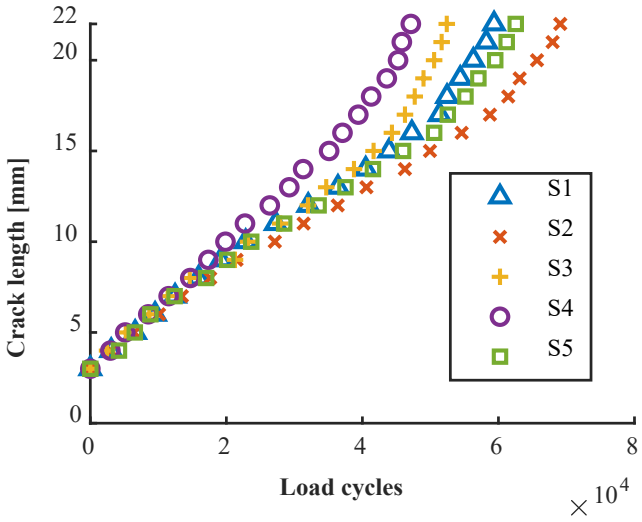

Fig. 3. Crack growths of specimens S1 ~ S5.

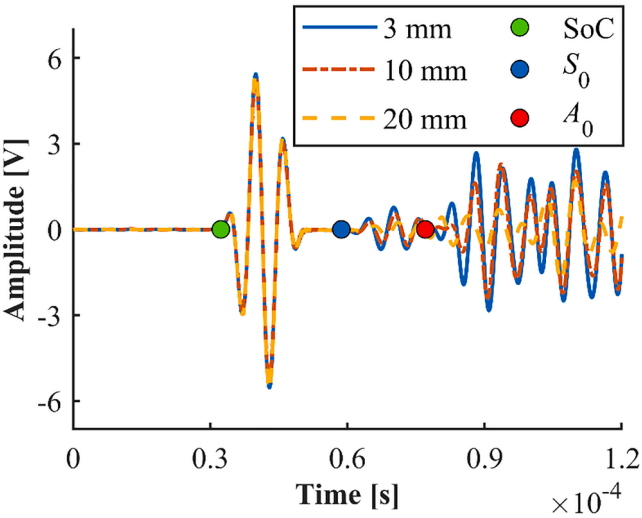

Fig. 4. Lamb wave signals at three crack lengths from specimen S5. Note: 'SoC' means 'start of crosstalk'.

finally Section 3.5 illustrates the target crack growths and their corresponding features using all the experimental specimens.

3.1. Experimental study

Fig. 2 (a) and (b) show the fatigue tests of the lug joint aluminum structure and a Lamb wave-based monitoring system [28], respectively. The thickness of the specimen and the diameter of the through hole are 5mm and 25mm, respectively. One 2mm long notch is created at the edge of the hole to initiate the crack growth. The MTS810 electro-hydraulic servo material test system is employed to provide the sinusoidal tensile fatigue load, whose maximum value, load ratio, and frequency are 18kN, 0.1, and 10Hz, respectively.

Fig. 2 (c) presents the crack on the specimen surface observed by a digital microscope. The scale lines are equally spaced by 1mm. A pre-cracking step is performed at the beginning of the fatigue test until the crack length reaches 3mm. The fatigue loading is occasionally paused during the test, and an 18kN static tensile load is applied to the structure to open the crack for better visualization. The crack length is considered to increase by 1mm once the crack tip reaches the next line.

Fig. 3 shows the fatigue crack growth trajectories of the five specimens S1–S5. Their differences are mainly caused by the uncertainties arising from the material property, specimen assembling, external loading condition, etc., which confirms that a deterministic damage evolution model can hardly provide accurate prognostic results. The crack lengths of 3mm and 22mm are taken as the initial crack and the threshold for RUL calculation, respectively.

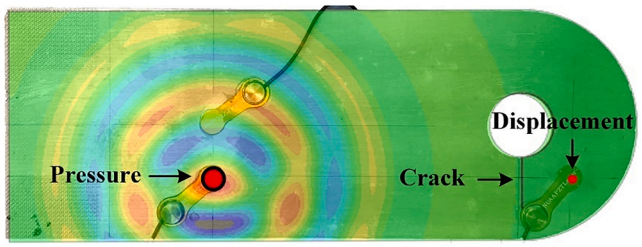

Fig. 5. Numerical setup.

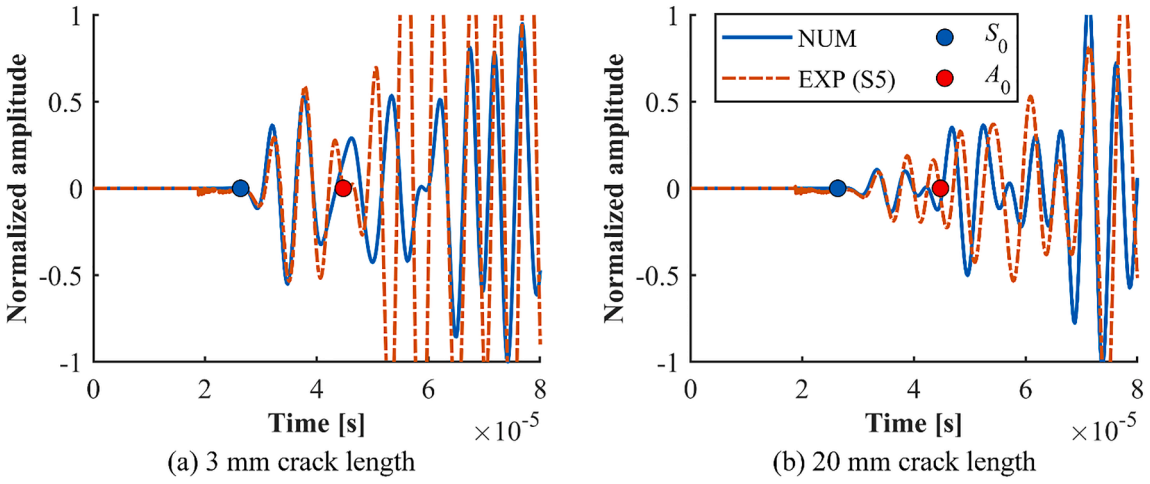

Fig. 6. Numerical and experimental (specimen S5) Lamb waves at two crack lengths.

Fig. 2 (b) shows the piezoelectric transducers used as actuator and sensor in this study. At each measured crack length, the actuator provides a 3-cycle Hanning-windowed sine burst with a central frequency of 160kHz, and the sensor collects the Lamb wave with a sampling frequency of 50MHz.

Fig. 4 compares the experimental Lamb waves at three different crack lengths over a time window of 1.2×10^{-4}s, where the green, blue, and red dots represent the start of crosstalk (SoC), the analytical S_0 and A_0 arrivals, respectively. The first (fictitious) wave packet is a crosstalk arising from the electromagnetic induction between the actuator and sensor circuits, so the start of the crosstalk (SoC) is approximately equivalent to the time at which the excitation from the actuator is applied to the structure [26]. The analytical S_0 arrival is approximated by the summation of the SoC and its wave time-of-flight, and so is the analytical A_0 arrival. The interested reader may refer to [7] for more details. The second wave package is the S_0 mode wave. A good match can be found between the calculated and actual S_0 arrivals. The increasing crack lengths induce amplitude reductions of the S_0 waves, and consequently, the variation of the statistical feature extracted from those signals.

3.2. Numerical study

The numerical simulations of Lamb waves under different crack lengths [7] are introduced here, and they will be processed to provide some statistical features for modeling the measurement equation later. It is worth noting that such an equation can be formulated using Lamb waves obtained from either numerical simulations or experimental tests. In this study, numerical data is utilized for building the measurement equations, leaving all the experimental specimens for testing, thus allowing for a more comprehensive performance evaluation of the proposed method.

The interested reader may refer to [7] for more details of the simulations. Fig. 5 shows the results of an ABAQUS EXPLICIT simulation providing the numerical S_0 Lamb waves of the aluminum lug structure at nine crack lengths, i.e., $\{3, 5, 8, 10, 12, 15, 18, 20, 22\,\text{mm}\}$. Two symmetric out-of-plane pressures are applied within the 4 mm radius circles (shape of the actuator) on the two sides of the plate, whose amplitudes are the same as the excitation used in the experiment. The out-of-plane displacements at the center of the sensor location are taken as the numerical Lamb wave of reference.

Fig. 6 (a) and (b) show the comparisons of the numerical and experimental (specimen S5) Lamb waves at crack lengths of 3 mm and 20 mm, respectively. The crosstalk of the experimental signal is replaced by zero values for simplicity. The numerical S_0 Lamb waves satisfactorily agree with the experimental ones before 4×10^{-5}s, while the increasing differences after 4×10^{-5}s is related to multiple sources of uncertainty, e.g., the differences between the simulated and the actual cracks, and those between the wave modes of

Table 4
Four damage-sensitive statistical features used in this study.

Signal energy-based feature [33]	$F_{1,d} = 1 - \left\| \frac{cov(f_d, f_r)}{std(f_d)std(f_r)} \right\|$
Signal energy-based feature [34]	$F_{2,d} = \frac{\int (f_d(t), f_r(t))^2 dt}{\int (f_r(t))^2 dt}$
Peak-based feature	$F_{3,d} = 1 - \frac{max(f_d)}{max(f_r)}$
Root-mean-square (RMS) value-based feature	$F_{4,d} = 1 - \frac{rms(f_d)}{rms(f_r)}$

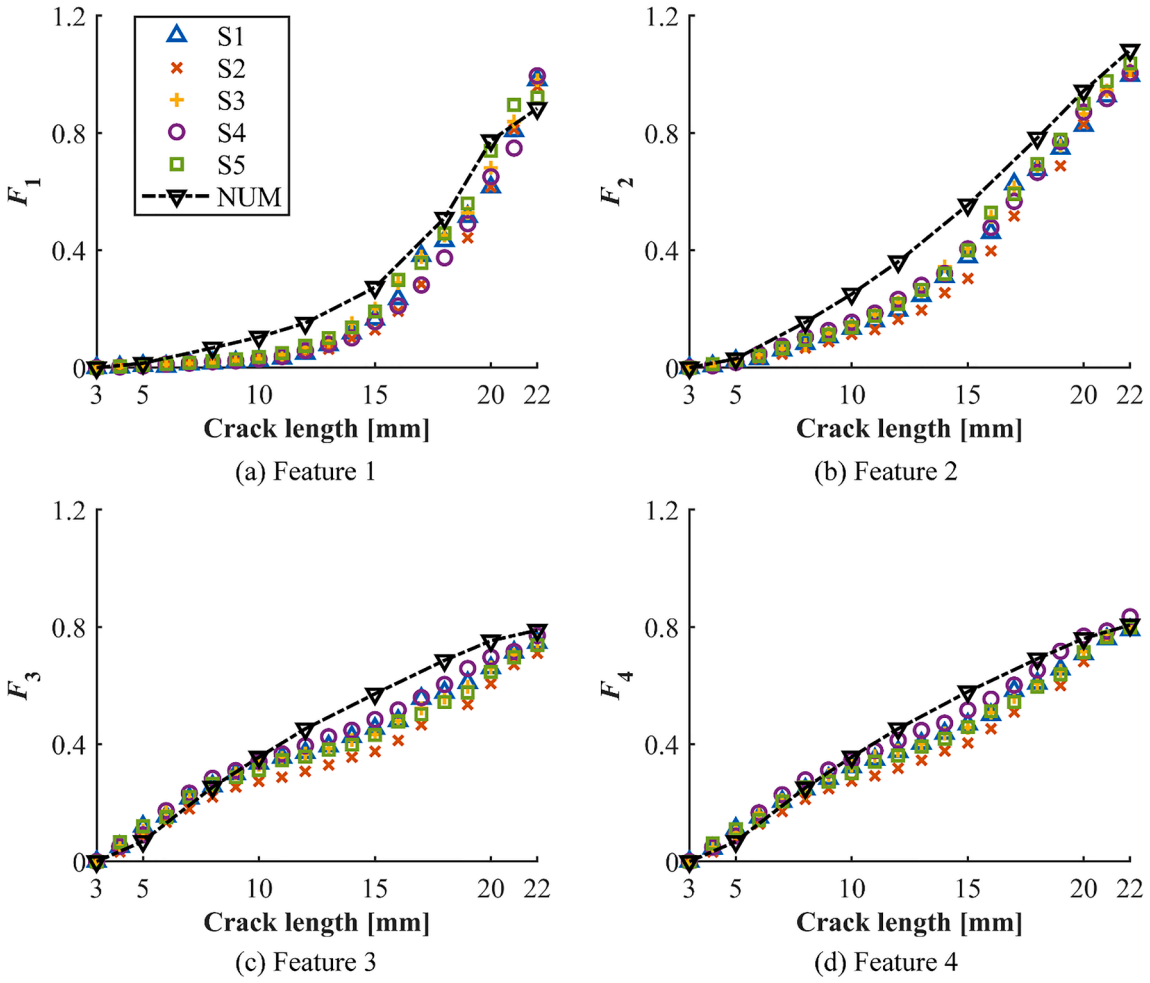

Fig. 7. Four damage-sensitive features at different crack lengths from numerical and experimental studies.

simulated (*S* mode only) and experimental (*S* and *A* modes) signal, as well as diverse boundary reflections.

3.3. Feature extraction

As already performed in [7], some damage-sensitive statistical features are extracted from the Lamb waves within a certain window, whose start and width are the S_0 arrival and 10^{-5}s, respectively. Table 4 shows the four features used in this study, and their performances for damage prognosis are demonstrated in [7,22,28]. Note that f_r and f_d are the windowed Lamb waves at the initial reference crack length of 3mm and another crack length d, respectively, t means the time instant, the function '*cov*' is the covariance of the Lamb waves f_r and f_d, and the functions '*std*', '*max*', '*rms*' are the standard deviation, peak value, and root-mean-square value of an individual set of signals, respectively.

Table 5
Coefficients of the 4-th order polynomial function for each feature fitted from numerical study.

		$p_1[\times 10^{-5}]$	$p_2[\times 10^{-3}]$	$p_3[\times 10^{-2}]$	$p_4[\times 10^{-1}]$	p_5
Model (i)	Feature 1	−2.309	1.230	−1.922	1.258	−0.248
Model (ii)	Feature 2	−0.181	0.022	0.266	0.008	−0.031
Model (iii)	Feature 3	0.571	−0.336	0.584	0.139	−0.092
Model (iv)	Feature 4	0.742	−0.420	0.727	0.044	−0.074

Table 6
Particle filter parameters.

Number of particles N_p	h in kernel smoothing	Standard deviation in likelihood function	
6000	0.1	0.02	
Initial distributions for $\ln C$ $\left[\ln\frac{\text{mm}}{\text{cycle}(\text{MPa}\sqrt{\text{mm}})^{-m}}\right]$, m [-]		Initial range for $\times$ [mm]	Initial value for b [-]
$\begin{bmatrix}\ln C_0\\ m_0\end{bmatrix} \mathcal{N}\left(\begin{bmatrix}-57.18\\ 8.101\end{bmatrix}, \begin{bmatrix}0.9966 & -0.1764\\ -0.1764 & 0.0346\end{bmatrix}\right)$		$x_0 \sim \text{U}(2.5, 3.5)$	$b_0 = 0$
Distributions of process noises $\{\omega, \omega_1, \omega_2, \omega_b\}$ for $\times$,ln$C$, m, b			
$\omega\ \mathcal{N}\left(-\frac{0.01^2}{2}, 0.01^2\right)$	$\omega_1\ \mathcal{N}(0, 0.01^2)$	$\omega_2\ \mathcal{N}(0, 0.001^2)$	$\omega_b\ \mathcal{N}(0, 0.005^2)$

The above feature extraction is carried out for the numerical and the experimental Lamb waves from each of the five specimens, as shown in Fig. 7. First, the monotonic upward trend between crack length and the features demonstrates that all four features are sensitive to crack growth. The satisfactory match between the numerical and experimental features allows the adoption of the numerical data for modeling the measurement equation, however, as mentioned above, the unavoidable bias (though small) might hamper a satisfactory prognosis. The features from experimental specimens S1–S5 will be processed in Section 3.5 for validating the proposed framework.

3.4. State space modeling and PF parameters

The crack propagation is described by the discrete form of Paris's law,

$$x_k = x_{k-1} + C(\Delta K(x_{k-1}))^m \Delta N \tag{7}$$

where x is the crack length, the number of load cycles included at one time step ΔN is assumed to be known, the two empirical parameters C and m can be determined by conducting fatigue tests on standard specimens made of the same material, or obtained by conducting fatigue tests on one or several replicas of the same testing structure, and the stress intensity factor range ΔK at each crack length is fitted through some numerical simulations conducted by the same authors in [6]:

$$\Delta K(x) = 0.0014x^3 + 0.5626x^2 - 13.50x + 497.8 \tag{8}$$

Then, the bias-based prognostic model for the l-th feature can be written as [6]:

$$\begin{cases} \boldsymbol{z}_{l,k} = \begin{bmatrix}\ln C_k\\ m_k\\ x_k\\ b_{l,k}\end{bmatrix} = \begin{bmatrix}\ln C_{k-1} + \omega_{1,k}\\ m_{k-1} + +\omega_{2,k}\\ x_{k-1} + e^{\omega_k} C_k(\Delta K(x_{k-1}))^{m_k}\Delta N\\ b_{l,k-1} + \omega_{l,b,k}\end{bmatrix} \\ y_{l,k} = g_l(x_k) + b_{l,k} + \nu_{l,k} \end{cases} \tag{9}$$

where $\omega\ \mathcal{N}\left(-\frac{\sigma^2}{2}, \sigma^2\right)$ is the unbiased Gaussian process noise with standard deviation σ [17], ω_1, ω_2 and ω_b are zero-mean Gaussian process noises, and the observed signal feature y can be one of those in Table 4.

The function $g_l(\bullet)$ is taken as a 4-th order polynomial fitting regression:

$$g_l(x) = p_1x^4 + p_2x^3 + p_3x^2 + p_4x + p_5 \tag{10}$$

There can be four independent prognostic models in this study, each sharing the same form of Eq. (9) but having its polynomial coefficients for $g_l(x)$ in Eq. (10). More specifically, coefficients $p_1, \cdots, p_5$ are fitted based on numerically simulated features (as a function of crack length), and they are given in Table 5.

Notice that Eq. (9) is taken as a nonlinear and non-Gaussian model, due to the non-linearities of Paris' law and the function $g(\bullet)$, and the non-Gaussian noise e^{ω}, respectively. Kernel smoothing [35] is adopted to improve the accuracy of estimating the time-invariant parameters ln C and m, through Eq. (11)

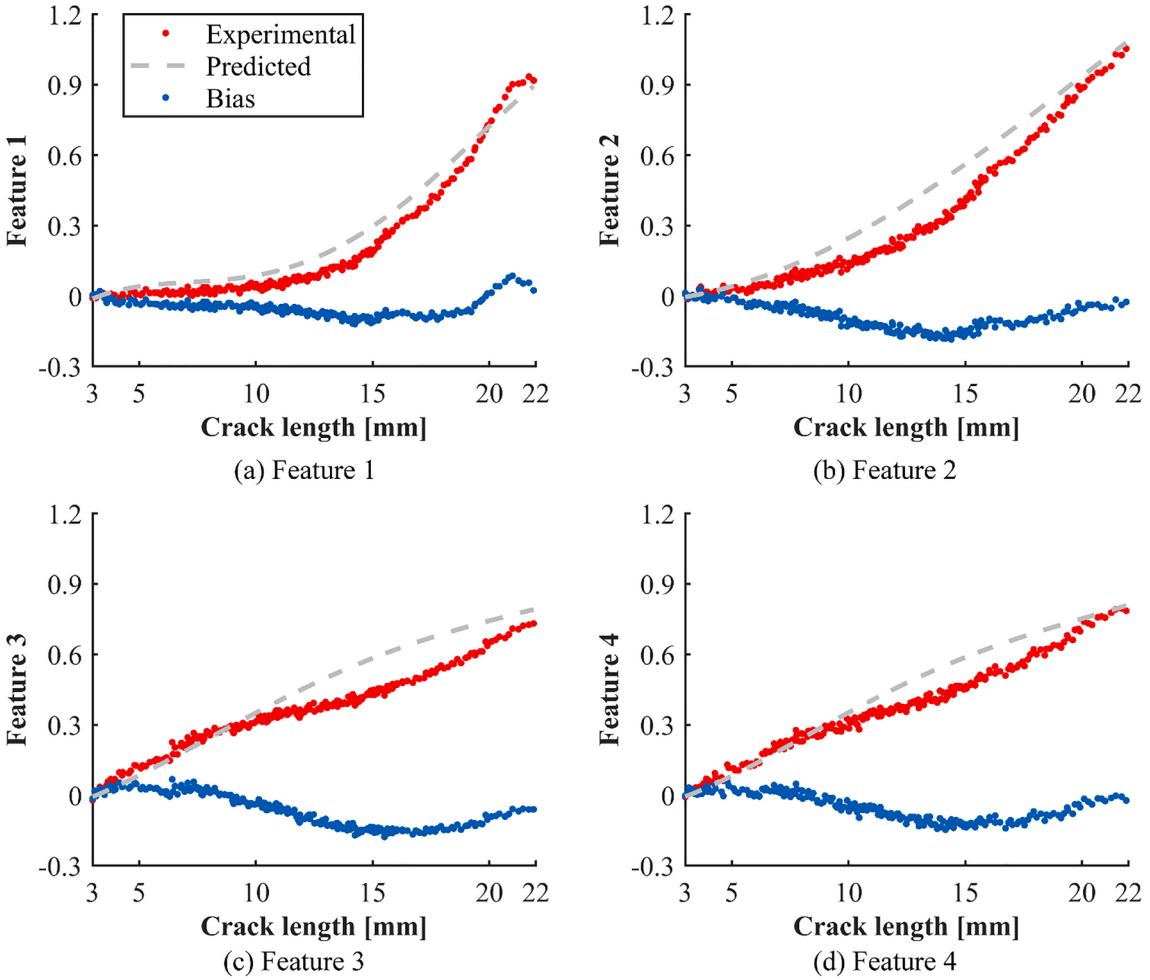

Fig. 8. Experimental and predicted features and bias at each crack length from specimen S5.

Table 7
Number of time steps of each feature being the best feature.

	Total number of time steps	Feature 1	Feature 2	Feature 3	Feature 4
Specimen S1	197	19	15	53	110
Specimen S2	230	109	5	47	69
Specimen S3	175	56	10	46	62
Specimen S4	157	6	19	34	98
Specimen S5	208	111	14	34	49

Note: the largest step number of one feature being the best for each specimen is highlighted in grey.

Table 8
Estimation and prognostic performances using one feature (traditional method) for specimen S5.

		Traditional method using one feature			
Selected feature		1	2	3	4
Performance metric	RMSE [mm]	0.863	1.289	0.906	1.091
	PH [Load cycles]	13,800	10,200	4800	6000
	CRA	0.631	0.413	0.644	0.602
Number of steps of each feature being the best / Number of total steps		111/208	14/208	34/208	49/208

Note: (i) the largest step number of one feature being the best feature is highlighted in grey; (ii) the smallest RMSE, largest PH, or highest CRA means the 'best' performance, and they are highlighted in green.

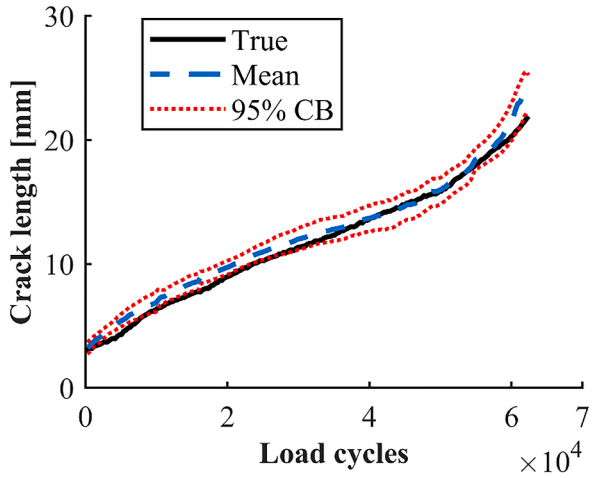

(a) Crack length estimation

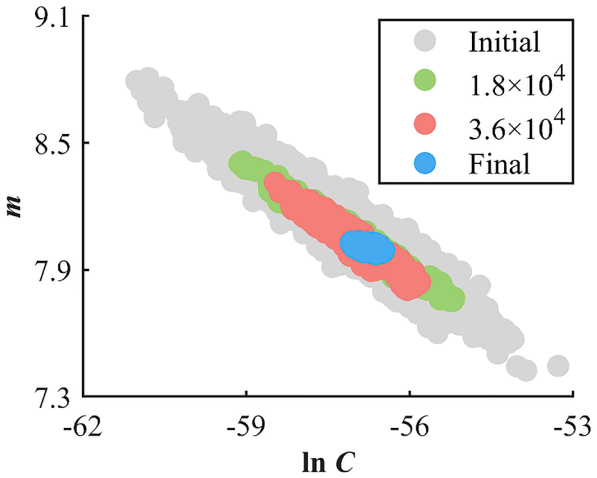

(b) Parameter estimation

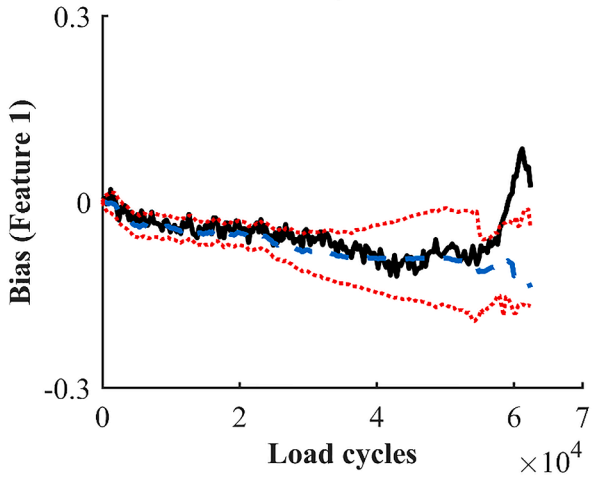

(c) Bias estimation - feature 1

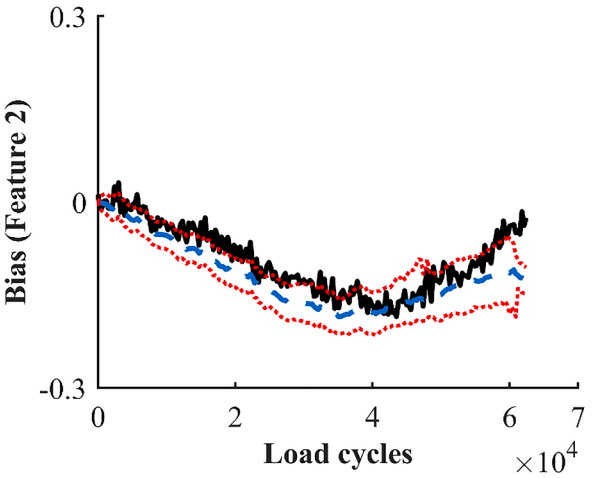

(d) Bias estimation - feature 2

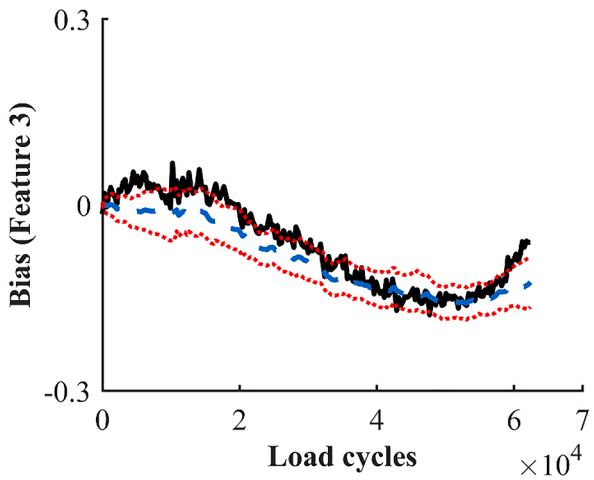

(e) Bias estimation - feature 3

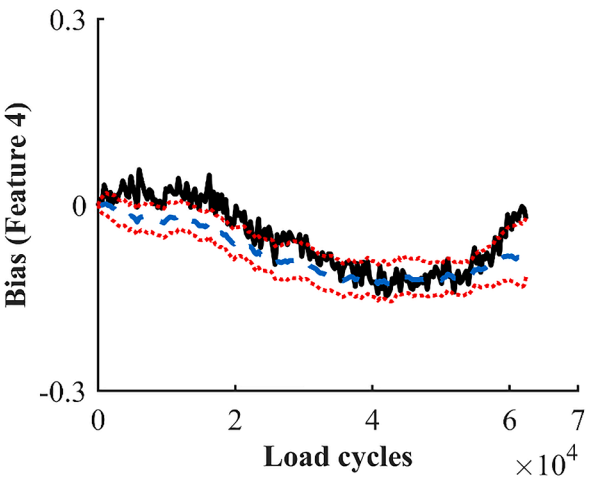

(f) Bias estimation - feature 4

Fig. 9. Estimation results using new method from specimen S5. Note: (i) Figures (a), (c), (d), (e) and (f) share the same legend, (ii) 'CB' means the confidence boundary; (iii) 'Initial', '1.8×10^4', '3.6×10^4', and 'Final' represent the samples of the three parameters at 0, 1.8×10^4, 3.6×10^4, and last load cycles, respectively.

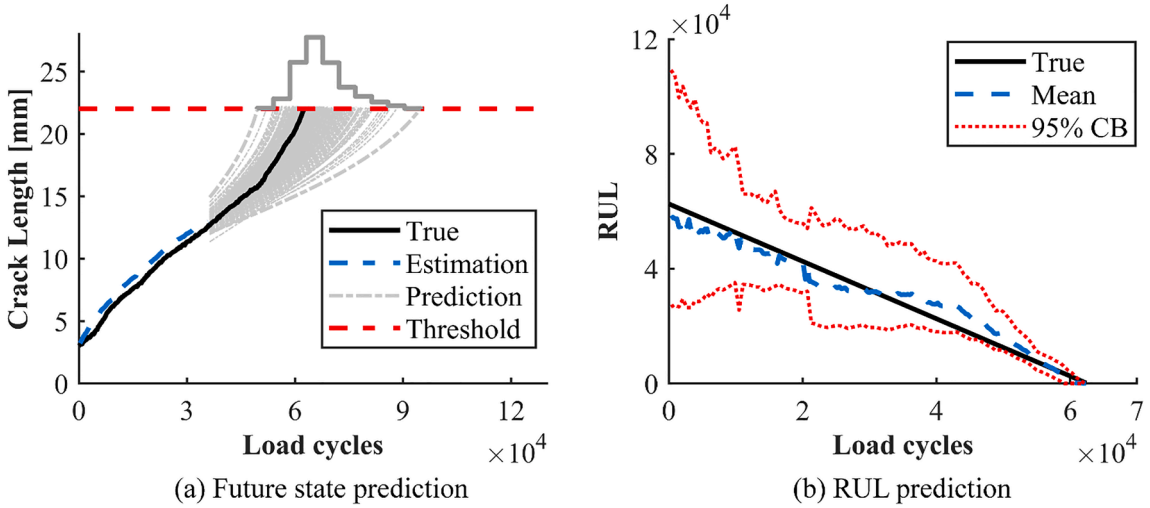

Fig. 10. Future state prediction at 3.6×10^4 load cycles and RUL prediction using new method from specimen S5.

Table 9
Estimation and prognostic performances by adopting one feature (traditional method) and by combining multiple features (new method) for specimen S5.

Selected feature		Traditional method using one feature				New method using four features	
		1	2	3	4	Use **true** bias to define best feature	Use **estimated** bias to define best feature
Performance metric	RMSE [mm]	0.863	1.289	0.906	1.091	0.604	0.727
	PH [Load cycles]	13,800	10,200	4800	6000	36,300	45,900
	CRA	0.631	0.413	0.644	0.602	0.837	0.835
Number of steps of each feature being the best / Number of total steps		111/ 208	14/ 208	34/ 208	49/ 208	–	–
Accuracy of using estimated bias to find the target best feature		–				–	114/208 (54.8%)

Note: (i) the largest step number of one feature being the best feature is highlighted in grey; (ii) the smallest RMSE, largest PH, or highest CRA means the 'best' performance, and they are highlighted in green; and (iii) the result from new method is highlighted in blue if it is more accurate than that from the traditional method. Same below.

$$\begin{cases} \ln C_k = \sqrt{1-h^2}\,\ln C_{k-1} + \left(1-\sqrt{1-h^2}\right)\widehat{\ln C}_{k-1} + \omega_{1,k} \\ m_k = \sqrt{1-h^2}\,m_{k-1} + \left(1-\sqrt{1-h^2}\right)\hat{m}_{k-1} + \omega_{2,k} \end{cases} \tag{11}$$

where the smoothing parameter h is a value within a range of $[\,0 \quad 1\,]$, and $\widehat{\ln C}$ and $\hat{m}$ are the means of the samples for the parameters $\ln C$ and m, respectively.

Table 6 shows the values of the PF parameters used in this study, most of which are determined based on the previous experiences of the same authors [6,7]. The four models above share the same PF parameters. The effects of these parameters on PF performances can be found in literature [2,36], thus is not discussed hereafter for simplicity.

3.5. Target crack growth and features

The available experimental crack lengths and the Lamb wave signals have been offline collected over a long-time interval (i.e., every several thousand load cycles), resulting in few observations and preventing an efficient convergence of the PF. To simulate an online SHM application scenario, where the Lamb waves can be collected at a higher frequency (or, equivalently, at shorter load cycle intervals) for crack length quantification, the crack growth and the features from each of the five experimental specimens are used to create the target crack lengths and the corresponding features through the procedure below [6,7]:

(i) Linearly interpolate the crack lengths from each specimen to create the target lengths every 300 load cycles, and corrupt the crack lengths by white Gaussian noise with a signal-to-noise ratio (SNR) of 50dB to simulate stochasticity in the crack growth

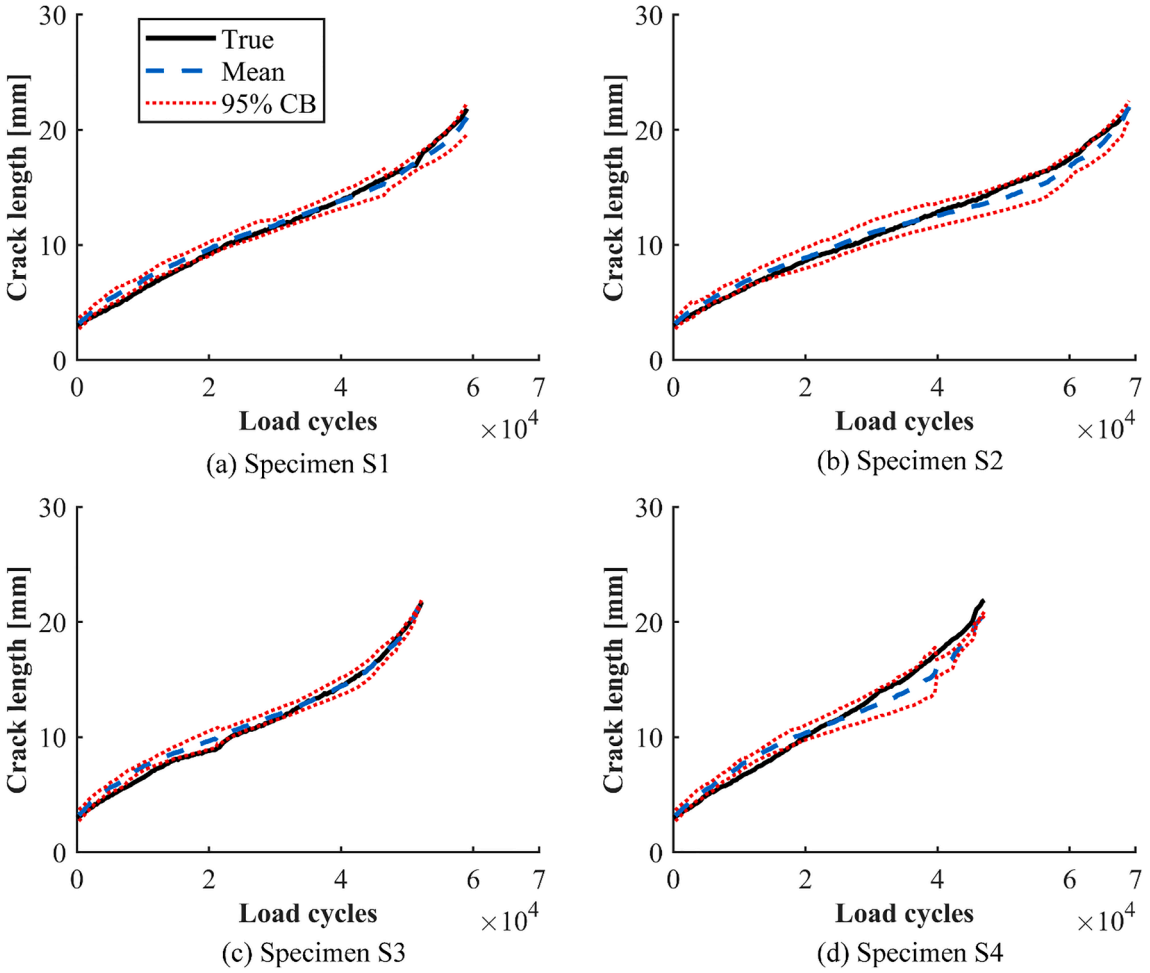

Fig. 11. Crack length estimations from new method for specimens S1 ~ S4.

process. Notice that, for these crack growth trajectories, we consider that no direct measurement has been applied during the degradation process, which represents the realistic situation in which the crack length can hardly be directly measured.

(ii) For each specimen, use linear interpolation to assign the four features at each created crack length, and corrupt these features by white Gaussian noise with a SNR of 30dB to simulate the measurement noise.

Fig. 8 shows the target experimental and predicted (by the function $g_l(\bullet)$) feature measurements from specimen S5, confirming that the bias from any feature is time-varying and different. Note that, in this study, the true bias at one step is taken as the smallest absolute value of bias at that step and the feature with the smallest true bias is taken as the target best feature. Table 7 lists the number of time steps each feature results in the best in tracking each specimen degradation. Here we remark the best feature for one specimen is not guaranteed to be the most performing for another one, indicating that the traditional method resorting to one feature may result in different prognostic performances for different specimens. Moreover, each of the four features can be the best only at specific steps for the same specimen (and not during the entire degradation process), which proves the need for an integrated framework for online fusing and selecting the best feature.

4. Application results

Results of the new approach based on feature fusion are described hereafter, applied to all five experimental specimens, and compared to those from the traditional approach based on a single feature. Sections 4.1 and 4.2 present the results by the traditional method separately resorting to each of the four features and by the new approach with feature fusion and selection, respectively, focused on specimen S5. The performances of the two methods on all the other specimens are synthesized in Section 4.3.

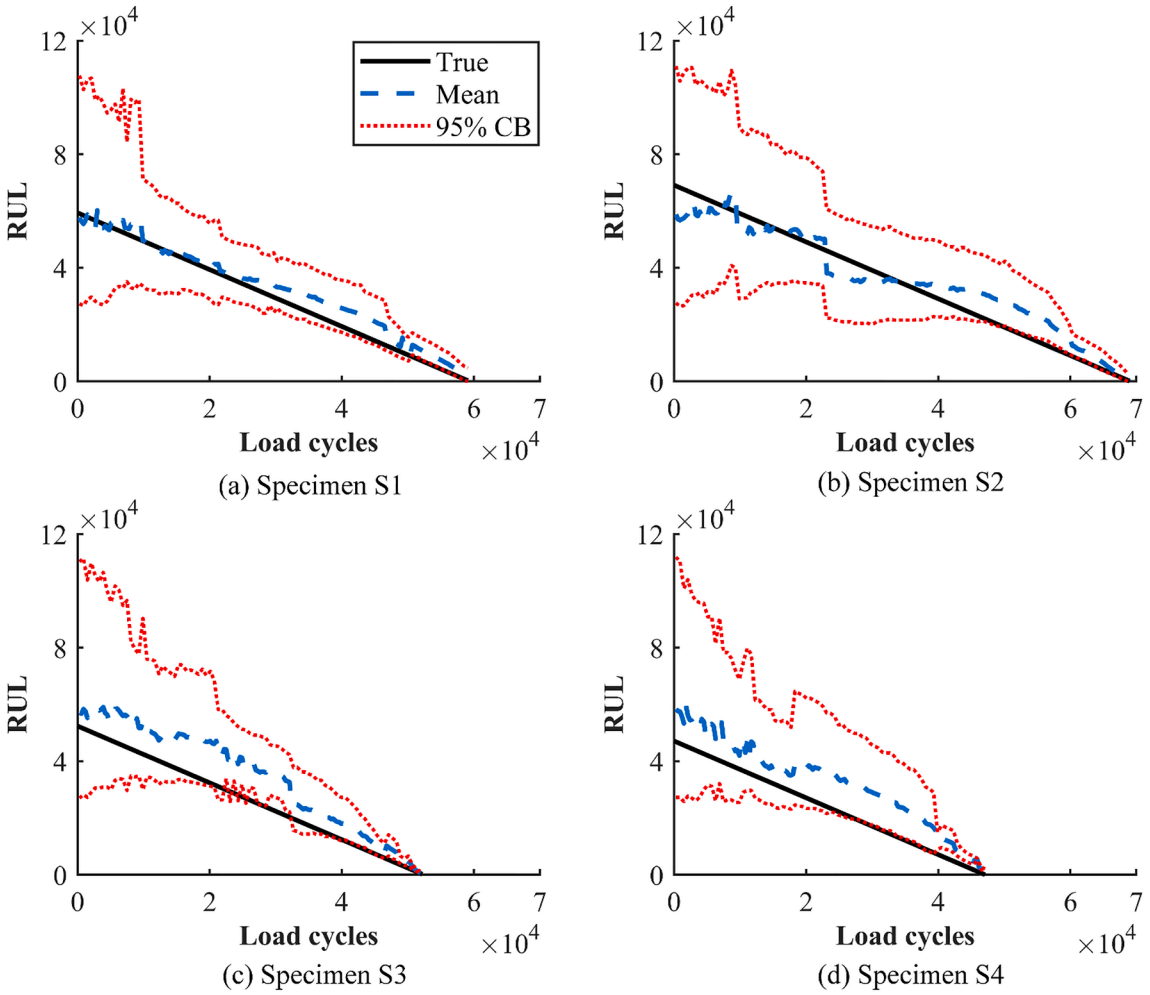

Fig. 12. RUL predictions from new method for specimens S1 ~ S4.

Table 10
Estimation and prognostic performances by adopting one feature (traditional method) and by combining multiple features (new method) for specimen S1.

Which feature to be used		Traditional method using one feature				New method using four features	
		1	2	3	4	Use **true** bias to define best feature	Use **estimated** bias to define best feature
Performance metric	RMSE [mm]	0.903	1.582	1.011	0.890	0.276	0.505
	PH [Load cycles]	9900	8400	3900	4800	33,000	41,400
	CRA	0.556	0.112	0.479	0.594	0.798	0.747
Number of steps of each feature being the best one / Number of total steps		19/ 197	15/ 197	53/ 197	110/ 197	–	–
Accuracy of using estimated bias to find the target best feature		–				–	110/197 (55.8%)

Note: (i) the largest step number of one feature being the best feature is highlighted in grey; (ii) the smallest RMSE, largest PH, or highest CRA means the 'best' performance, and they are highlighted in green; and (iii) the result from new method is highlighted in blue if it is more accurate than that from the traditional method. Same below.

Table 11
Estimation and prognostic performances by adopting one feature (traditional method) and by combining multiple features (new method) for specimen S2.

Which feature to be used		Traditional method using one feature				New method using four features	
		1	2	3	4	Use **true** bias to define best feature	Use **estimated** bias to define best feature
Performance metric	RMSE [mm]	0.962	1.744	1.401	1.773	0.853	0.568
	PH [Load cycles]	7500	10,500	1800	4800	44,700	35,700
	CRA	0.606	0.206	0.275	0.289	0.802	0.752
Number of steps of each feature being the best one / Number of total steps		109/ 230	5/230	47/ 230	69/ 230	–	–
Accuracy of using estimated bias to find the target best feature		–				–	176/230 (76.5%)

Table 12
Estimation and prognostic performances by adopting one feature (traditional method) and by combining multiple features (new method) for specimen S3.

Which feature to be used		Traditional method using one feature				New method using four features	
		1	2	3	4	Use **true** bias to define best feature	Use **estimated** bias to define best feature
Performance metric	RMSE [mm]	0.597	1.466	1.204	0.973	0.523	0.514
	PH [Load cycles]	6600	600	1200	2100	29,400	9300
	CRA	0.267	−0.301	0.043	0.282	0.782	0.605
Number of steps of each feature being the best one / Number of total steps		56/ 174	10/ 174	46/ 174	62/ 174	–	–
Accuracy of using estimated bias to find the target best feature		–				–	104/174 (59.8%)

Table 13
Estimation and prognostic performances by adopting one feature (traditional method) and by combining multiple features (new method) for specimen S4.

Which feature to be used		Traditional method using one feature				New method using four features	
		1	2	3	4	Use **true** bias to define best feature	Use **estimated** bias to define best feature
Performance metric	RMSE [mm]	1.298	1.500	1.349	1.107	0.888	0.934
	PH [Load cycles]	6300	6000	300	3900	4500	4500
	CRA	0.192	0.021	0.054	0.434	0.497	0.361
Number of steps of each feature being the best one / Number of total steps		6/ 157	19/ 157	34/ 157	98/ 157	–	–
Accuracy of using estimated bias to find the target best feature		–				–	75/157 (47.8%)

4.1. Application of traditional method (specimen S5)

For the traditional method, four particle filter (PF) routines are independently applied to the four prognostic models, each based on a single observed feature, thus resulting in four estimates of crack lengths, of parameters $\ln C$ and m, and of the measurement bias, as plotted in Figs. A.1, A.2, and A.3, respectively. In general, given the rather satisfactory bias estimation, the posterior PDF of the crack length based on each feature has its means remaining close to the target values, and also the samples corresponding to the parameters $\ln C$ and m are reducing their spread while more observations are processed and finally accumulate around some target values. However, their error, though apparently small, will result in a non-robust prognostic performance, as visible in Fig. A.5.

The predicted future states at 3.6×10^4 load cycles are given in Fig. A.4, where the predicted future states are distributed around the true crack lengths. This is also apparent in the RUL prediction of Fig. A.5, where the mean of RUL is close to the target RUL, and the confidence boundaries shrink with the increasing load cycle steps. The above observations are the same as those in [3,6]. However, due to the different bias levels among the four features, their overall performances are noted different, especially in RUL assessment, thus calling for a strategy of maximizing the use of best features to enhance the prognostic accuracy.

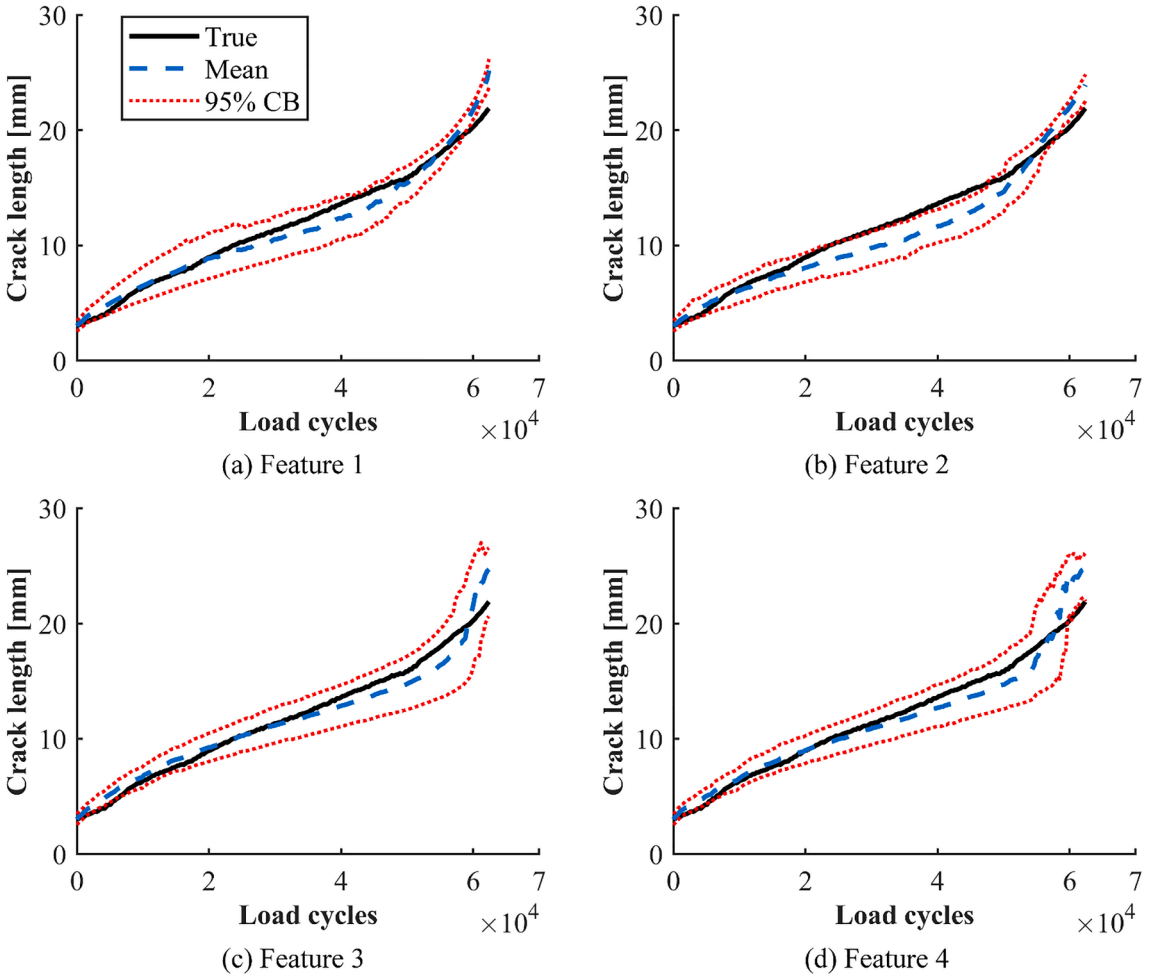

Fig. A1. Crack length estimation using traditional method resorting to one feature for specimen S5. Note: 'CB' means the confidence boundary.

To explore the relationship between the bias level and the diagnostic/prognostic performances, the results are processed by three metrics, i.e., the root-mean-square error (RMSE) of the crack length estimate, Eq. (12), the cumulative relative accuracy (CRA) of the RUL, Eq. (13), and the prognostic horizon (PH), i.e.,

$$RMSE = \sqrt{\frac{1}{T}\sum_{k=1}^{T}\left(\overline{x}_k - x_{true,k}\right)^2} \tag{12}$$

$$CRA = \frac{1}{T-1}\sum_{k=1}^{T-1}\left(1 - \frac{\left|\overline{RUL}_k - RUL_{true,k}\right|}{RUL_{true,k}}\right) \tag{13}$$

where $\overline{x}$ and $\overline{RUL}$ denote the posterior estimates of the crack length and of the RUL, respectively, the subscript '*true*' means the true crack length or RUL, and T is the number of discrete load cycle steps required by the PF until failure is reached.

PH is defined as the difference between the load cycle step at which the prediction meets desired criteria [37] and the end-of-life. The end-of-life is considered as the end of the test, i.e., the number of load cycles N, and the PH is the distance between the number of load cycles when 60% of the RUL distribution falls within a range of 'true RUL $\pm$ 10%N' [17] and the end-of-life. Lower RMSE, higher CRA, and larger PH indicate better performances.

Table 8 presents the RMSEs, CRAs, and PHs from all specimens, where, despite the use of online estimation for compensating the measurement bias, the four features still yield different performances for the same specimen. In general, the feature being the best for the largest number of steps (i.e., the one having the smallest true bias) can provide the best prognostic performance. Any of the four features can be the best at specific time steps, justifying the effort in developing a scheme to maximize the adoption of the best features.

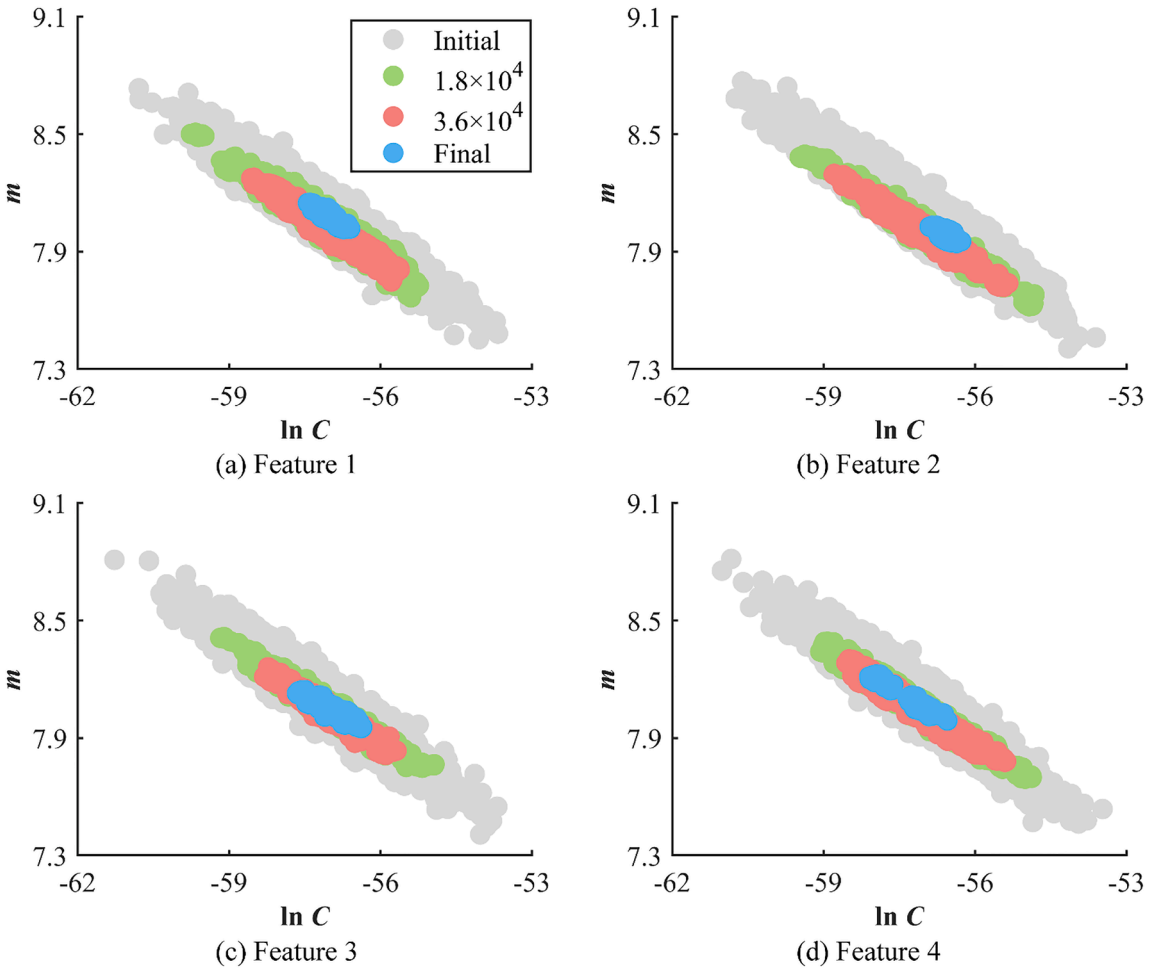

Fig. A2. Parameter estimation using traditional method resorting to one feature for specimen S5. Note that 'Initial', '1.8×10^4', '3.6×10^4', and 'Final' represent the samples of the three parameters at 0, 1.8×10^4, 3.6×10^4, and last load cycles, respectively.

4.2. Application of feature fusion and selection (specimen S5)

The newly proposed PF scheme combines the four prognostic models, each with a different observed feature. At each step, the best feature is defined as the one with the smallest estimated bias, and then the PF routine applies the best samples of crack length and its growth parameters for RUL prediction, and those of crack length for the one-step-ahead prediction by each prognostic model. Results are provided in Figs. 9 and 10 and Table 9. A separate PF routine is also considered for reference in Table 9, where the best feature is selected according to the true bias (not available in a real application but useful herein to assess the algorithm performance), instead of the predicted bias approximated by the PF.

Fig. 9 shows the bias estimates based on the fused features and the best estimates of crack length and its growth parameters, while Fig. 10 presents the relative future states and RUL predictions. The conclusions about the mean values are generally similar to those arising from the figures in Appendix A.1, thus not repeated here. On the other hand, given that each feature can be the best one at specific time steps, the best samples of crack length have been selected among those of different features. As the range of those samples that have gone through four features should be smaller than that for one feature, the proposed method naturally brings to the narrower CBs of crack length, and consequently, RUL, compared with those from the traditional method. Due to the interconnection between the crack length and bias arising from the measurement equation, the bias also exhibits a more accurate estimation, demonstrating the superior capacity of the proposed method towards bias estimation.

Table 9 compares the performances of traditional and new methods. By adopting the true bias to select the best feature at each time step (note that this can hardly happen in reality and is just used as a reference for comparison), the new method always behaves better than the traditional one, confirming that the use of the bias-based best feature can improve the prognostic performance. There are still some estimation and prognostic errors because the true bias is not taken as a known constant in the state space model. When the estimated bias is used to define the best feature, a selection accuracy of 54.8% (114/208) is obtained, i.e., the proposed feature selection criterion is capable of finding the target best feature at 114 out of 208 time steps. However, the RMSE, PH, and CRA of the

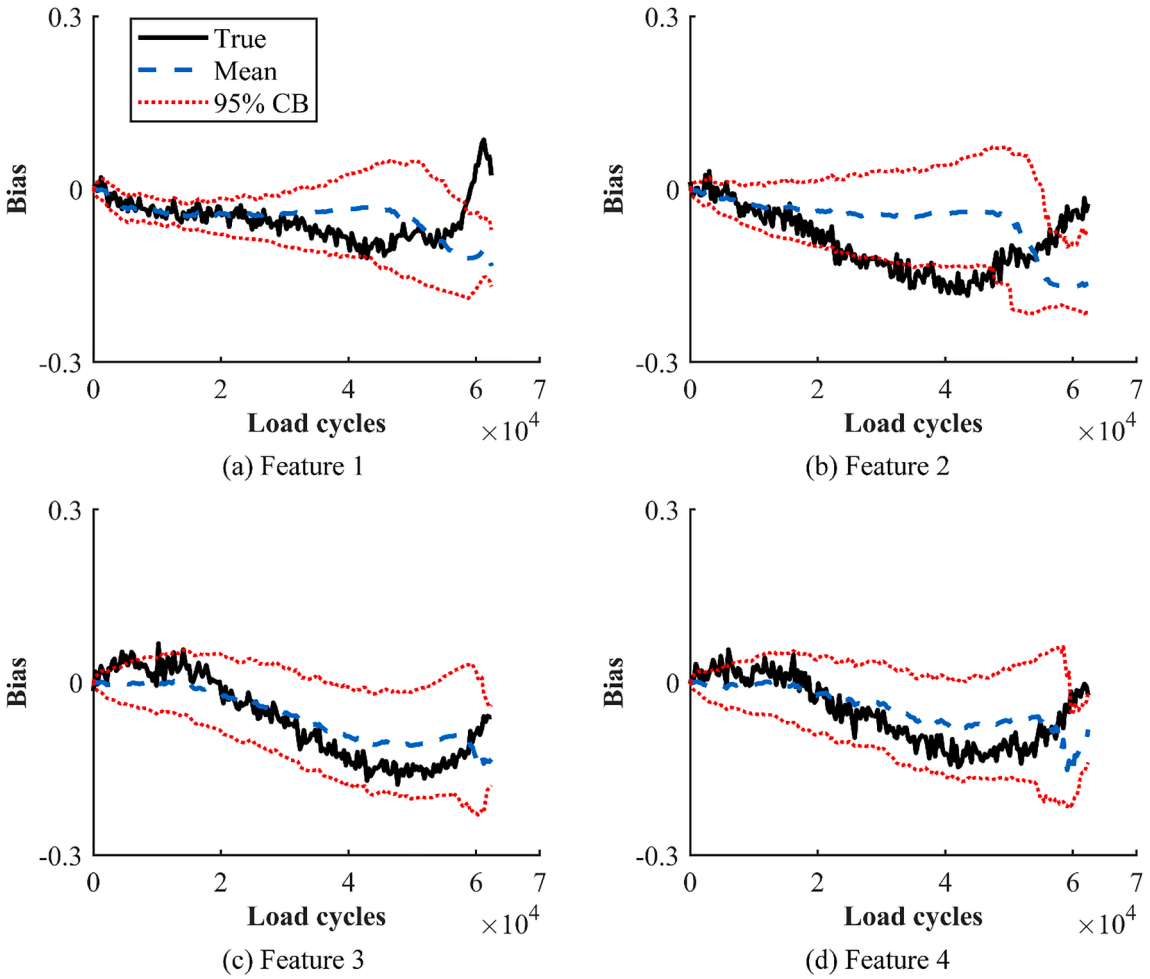

Fig. A3. Bias estimation using traditional method resorting to one feature for specimen S5.

proposed method are still more accurate than those of the traditional method using any of the four features.

One may be confused that Feature 1 has the most steps being the target best feature (111/208), and the performance of the traditional method resorting to that feature is much less accurate than that of the new method. A sudden bias variation from one feature like that of Feature 1 after 6×10^4 load cycles can hardly be accurately estimated, thus deteriorating the damage quantification performance, as shown in Fig. A.3. On the other hand, the new method always relies on different features providing the crack length samples for prior calculation at different steps, thus being less sensitive to such variation.

4.3. Results from all the other specimens

The robustness of the proposed framework is tested with the specimens S1–S4. The analyses in Sections 4.1 and 4.2 are repeated with the same PF parameters given in Section 3.4. The crack length estimation and RUL prediction results using the new method are presented in Figs. 11 and 12, respectively, which lead to the same conclusions drawn from Figs. 9 and 10 relatively to Specimen S5, demonstrating the robustness of the proposed method over different specimens.

Tables 10–13 show the damage quantification and RUL prediction performances for specimens S1–S4, respectively. Similar conclusions from Sections 4.1 and 4.2 can be drawn here. One exception is for specimen S4, where the new method has the best crack length estimation but less satisfactory RUL prediction, possibly because of the unsatisfactory estimation of the parameters ln C and m, which calls for some sort of strategy for fast and robust parameter estimation and also a better initialization of those parameters.

5. Conclusions

Damage prognosis methods typically require a data-driven measurement equation to describe the relationship between the damage state and some properly chosen damage-sensitive statistical features. As the best feature can vary for different specimens, or even, at different time steps for the same specimen, the selection of such a feature can hardly be a trivial task but has received little attention in

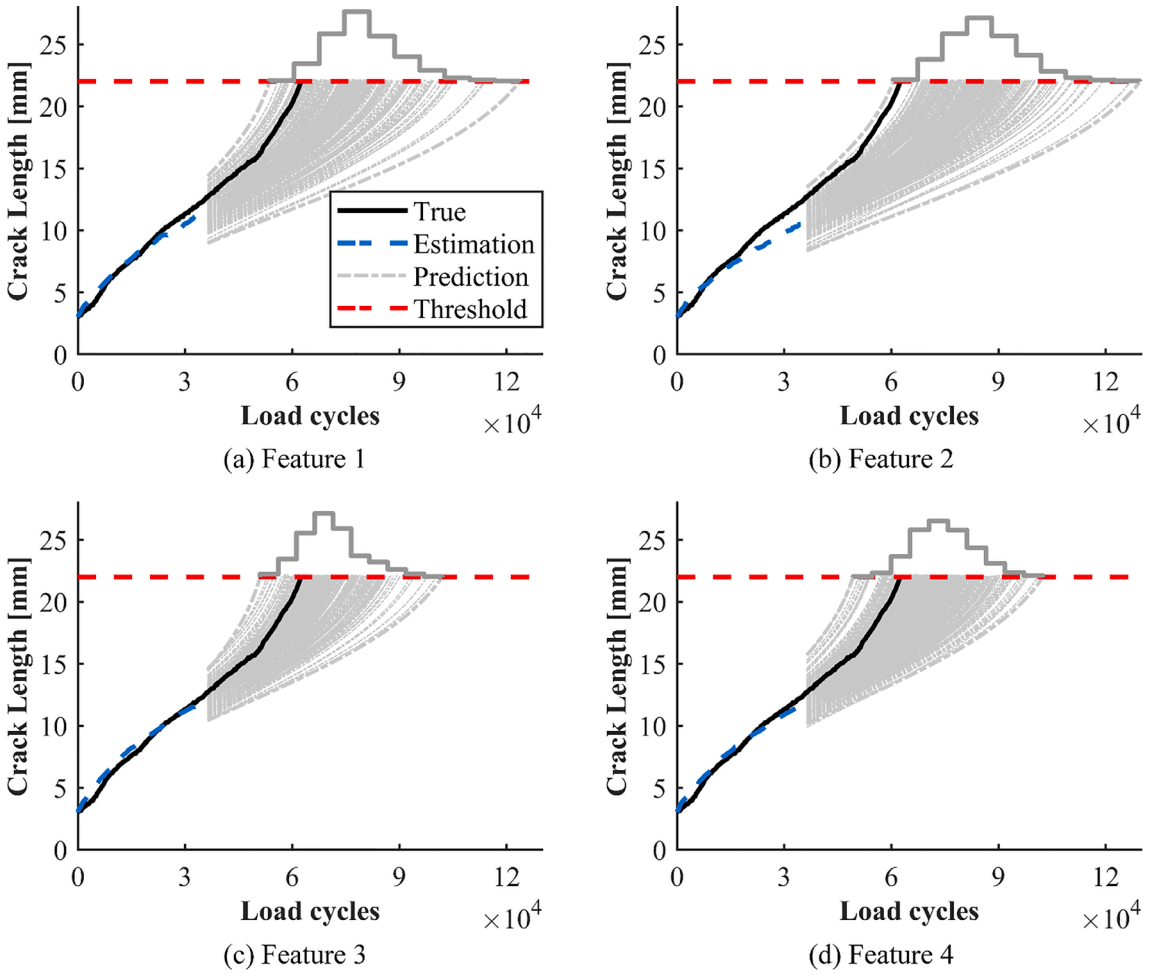

Fig. A4. Future state prediction at 3.6×10^4 load cycles using traditional method resorting to one feature for specimen S5.

current practices. By combining a novel online feature fusion and selection scheme with multiple prognostic models considering measurement bias, this work has proposed a new particle filter-based damage prognosis framework, where, at each step, the feature with the smallest estimated bias is taken as the best feature providing the best estimates at that step.

The results of the new method have been compared with the traditional approach, where the prognostic model resorting to one feature has been processed through one PF for damage quantification and RUL prediction. The traditional method has shown performance dependence on the feature choice. The smaller bias one feature has, the better performance it can provide, as a smaller bias can be more accurately estimated, having less effect on the estimation of the crack length. Any feature can be the best feature at specific steps, and the proposed method maximizes the use of the best features, thus yielding more accurate estimation and prognostic performances.

To move towards a more practical and robust application, one may consider three potential paths, from the perspectives of degradation modeling, feature fusion, and feature selection.

- This method exclusively relies on Paris's law for degradation modeling, without considering uncertainties stemming from factors such as the calculation of stress intensity factor and fatigue cycle counting. Consequently, the prognostic performance can be improved by incorporating additional uncertainties into the prognostic model. Moreover, one can explore the fusion of multiple physics-based and data-driven models to create a group of better-distributed damage state samples as prior and then to enhance the estimation and prognostic performance.
- This method is only validated in a case study where some statistical features are extracted from Lamb wave signals, specifically by the same piezoelectric transducer. However, practical monitoring scenarios usually have multiple transducers and different types of sensors, like strain gauges and accelerometers, installed, resulting in different statistical and physics-related features. Due to the potentially significant variations in sensitivity and scale (or bias level) among these features, feature fusion remains a significant challenge.

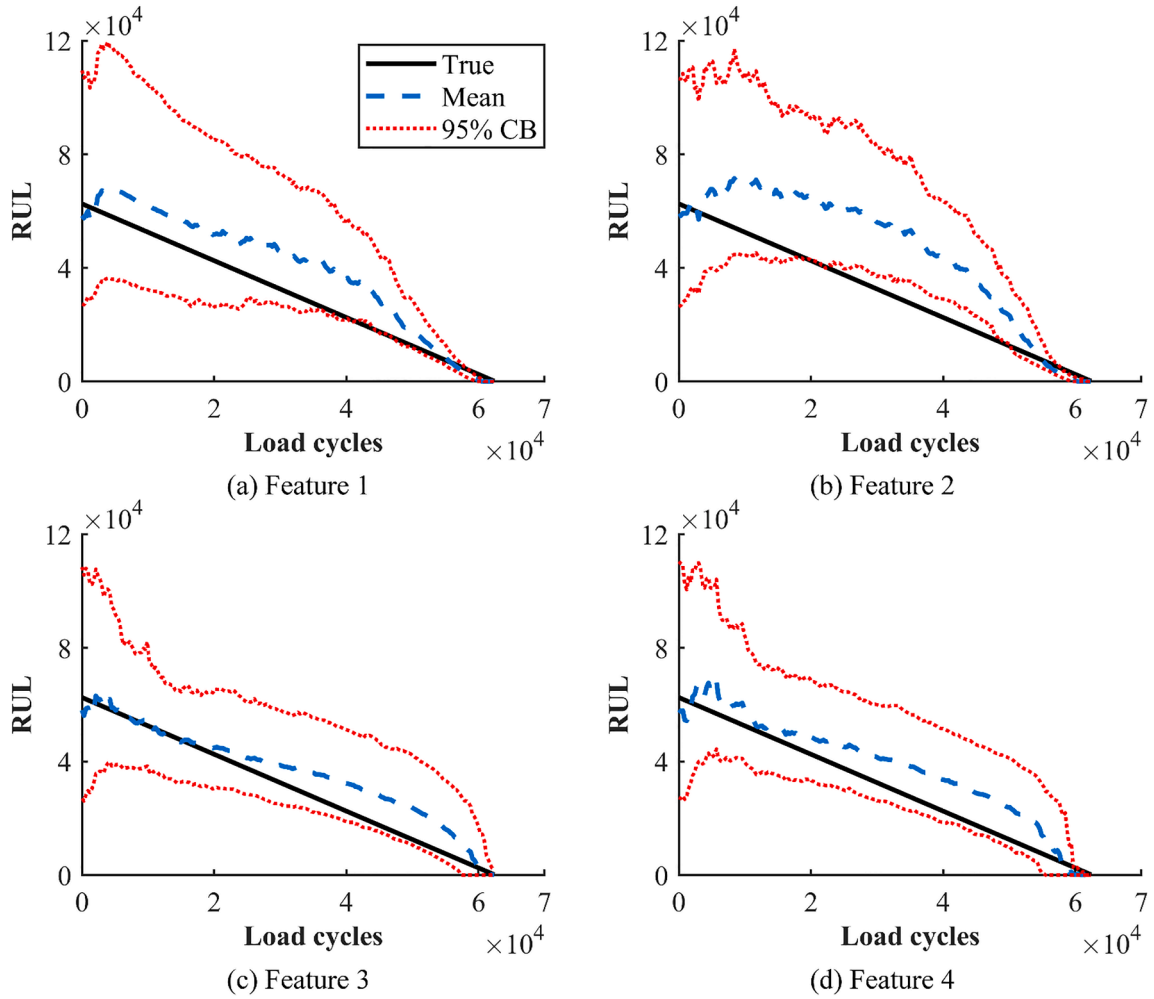

Fig. A5. RUL prediction using traditional method resorting to one feature for specimen S5.

- This method only resorts to the bias parameter for selecting the best feature at each step. The performance of PF-based estimation can be evaluated by other coefficients like the effective sample size, which could be also exploited for selecting the best feature. Furthermore, rather than always resorting to the particles from the best feature, different groups of particles can be weighted by the above coefficients and then applied to prior calculation, improving the particle diversity and possibly yielding a more robust prognostic performance.

Declaration of Competing Interest

The authors declare that they have no known competing financial interests or personal relationships that could have appeared to influence the work reported in this paper.

Data availability

Data will be made available on request.

Acknowledgments

This project has received funding from the European Union's Horizon 2020 research and innovation programme under the Marie Skłodowska-Curie grant agreement No. 859957.

Appendix A.1

The damage estimation and prognostic results for the traditional method (by using each of the four features separately) applied to specimen S5 are shown in Figs. A.1–A.5, specifically for crack length estimation, crack growth parameter estimation ($\ln C$ and m), bias estimation, future state prediction, and the RUL prediction, respectively.

References

[1] M. Chiachío, J. Chiachío, S. Sankararaman, K. Goebel, J. Andrews, A new algorithm for prognostics using Subset Simulation, Reliab. Eng. Syst. Saf. 168 (2017) 189–199.
[2] D. Cristiani, C. Sbarufatti, M. Giglio, Damage diagnosis and prognosis in composite double cantilever beam coupons by particle filtering and surrogate modelling, Struct. Health Monit. (2020), 1475921720960067.
[3] T. Li, F. Cadini, M. Chiachío, J. Chiachío, C. Sbarufatti, Particle filter-based delamination shape prediction in composites subjected to fatigue loading, Struct. Health Monit. (2022), 14759217221116041.
[4] N. Yue, A. Broer, W. Briand, M. Rébillat, T. Loutas, D. Zarouchas, Assessing stiffness degradation of stiffened composite panels in post-buckling compression-compression fatigue using guided waves, Compos. Struct. 293 (2022), 115751.
[5] C. Tao, C. Zhang, H. Ji, J. Qiu, Application of neural network to model stiffness degradation for composite laminates under cyclic loadings, Compos. Sci. Technol. 203 (2021), 108573.
[6] T. Li, C. Sbarufatti, F. Cadini, J. Chen, S. Yuan, Particle filter-based hybrid damage prognosis considering measurement bias, Strct. Control Health Monitor. n/a (2021) e2914.
[7] T. Li, L. Lomazzi, F. Cadini, C. Sbarufatti, J. Chen, S. Yuan, Numerical simulation-aided particle filter-based damage prognosis using Lamb waves, Mech. Syst. Sig. Process. 178 (2022), 109326.
[8] J. Chen, S. Yuan, C. Sbarufatti, X. Jin, Dual crack growth prognosis by using a mixture proposal particle filter and on-line crack monitoring, Reliab. Eng. Syst. Saf. 215 (2021), 107758.
[9] F. Zhao, X. Zhou, C. Wang, L. Dong, S.N. Atluri, Setting adaptive inspection intervals in helicopter components, AIAA J. 61 (6) (2023) 2675–2688.
[10] X. Zhou, S. He, L. Dong, S.N. Atluri, Real-time prediction of probabilistic crack growth with a helicopter component digital twin, AIAA J. 60 (2022) 2555–2567.
[11] N. Eleftheroglou, D. Zarouchas, R. Benedictus, An adaptive probabilistic data-driven methodology for prognosis of the fatigue life of composite structures, Compos. Struct. 245 (2020), 112386.
[12] M. Moradi, A. Broer, J. Chiachío, R. Benedictus, T.H. Loutas, D. Zarouchas, Intelligent health indicator construction for prognostics of composite structures utilizing a semi-supervised deep neural network and SHM data, Eng. Appl. Artif. Intel. 117 (2023), 105502.
[13] G. Galanopoulos, N. Eleftheroglou, D. Milanoski, A. Broer, D. Zarouchas, T. Loutas, A novel strain-based health indicator for the remaining useful life estimation of degrading composite structures, Compos. Struct. 306 (2023), 116579.
[14] J. Fernández, M. Chiachío, J. Chiachío, R. Muñoz, F. Herrera, Uncertainty quantification in neural networks by approximate Bayesian computation: application to fatigue in composite materials, Eng. Appl. Artif. Intel. 107 (2022) 104511.
[15] P. Baraldi, F. Mangili, E. Zio, Investigation of uncertainty treatment capability of model-based and data-driven prognostic methods using simulated data, Reliab. Eng. Syst. Saf. 112 (2013) 94–108.
[16] I. Lopez, N. Sarigul-Klijn, A review of uncertainty in flight vehicle structural damage monitoring, diagnosis and control: challenges and opportunities, Prog. Aerosp. Sci. 46 (7) (2010) 247–273.
[17] M. Corbetta, C. Sbarufatti, M. Giglio, M.D. Todd, Optimization of nonlinear, non-Gaussian Bayesian filtering for diagnosis and prognosis of monotonic degradation processes, Mech. Syst. Sig. Process. 104 (2018) 305–322.
[18] F. Cadini, L. Lomazzi, M. Ferrater Roca, C. Sbarufatti, M. Giglio, Neutralization of temperature effects in damage diagnosis of MDOF systems by combinations of autoencoders and particle filters, Mech. Syst. Sig. Process. 162 (2022), 108048.
[19] M. Corbetta, C. Sbarufatti, M. Giglio, A. Saxena, K. Goebel, A Bayesian framework for fatigue life prediction of composite laminates under co-existing matrix cracks and delamination, Compos. Struct. 187 (2018) 58–70.
[20] T. Loutas, N. Eleftheroglou, D. Zarouchas, A data-driven probabilistic framework towards the in-situ prognostics of fatigue life of composites based on acoustic emission data, Compos. Struct. 161 (2017) 522–529.
[21] X. Liu, Y. Lei, N. Li, X. Si, X. Li, RUL prediction of machinery using convolutional-vector fusion network through multi-feature dynamic weighting, Mech. Syst. Sig. Process. 185 (2023), 109788.
[22] S. Buchaiah, P. Shakya, Bearing fault diagnosis and prognosis using data fusion based feature extraction and feature selection, Measurement 188 (2022), 110506.
[23] D. Cristiani, C. Sbarufatti, F. Cadini, M. Giglio, Fatigue damage diagnosis and prognosis of an aeronautical structure based on surrogate modelling and particle filter, Structural Health Monitoring, 0 1475921720971551.
[24] J. Chen, S. Yuan, X. Jin, On-line prognosis of fatigue cracking via a regularized particle filter and guided wave monitoring, Mech. Syst. Sig. Process. 131 (2019) 1–17.
[25] W. Wu, M.K. Malik, S. Cantero-Chinchilla, T. Lawrie, W.J. Yan, G. Tanner, R. Remenyte-Prescott, D. Chronopoulos, Guided waves-based damage identification in plates through an inverse Bayesian process, Ultrasonics 125 (2022), 106773.
[26] D. Yang, H.R. Karimi, K. Sun, Residual wide-kernel deep convolutional auto-encoder for intelligent rotating machinery fault diagnosis with limited samples, Neural Netw. 141 (2021) 133–144.
[27] J. Tian, D. Han, M. Li, P. Shi, A multi-source information transfer learning method with subdomain adaptation for cross-domain fault diagnosis, Knowl.-Based Syst. 243 (2022), 108466.
[28] J. Chen, S. Yuan, H. Wang, On-line updating Gaussian process measurement model for crack prognosis using the particle filter, Mech. Syst. Sig. Process. 140 (2020), 106646.
[29] E. Rabiei, E. Droguett, M. Modarres, Fully adaptive particle filtering algorithm for damage diagnosis and prognosis, Entropy 20 (2) (2018) 100.
[30] D.i. Song, F. Xu, T. Ma, Crack damage monitoring for compressor blades based on acoustic emission with novel feature and hybridized feature selection, Struct. Health Monit. 21 (6) (2022) 2641–2656.
[31] A. Broer, G. Galanopoulos, R. Benedictus, T. Loutas, D. Zarouchas, Fusion-based damage diagnostics for stiffened composite panels, Struct. Health Monit. 21 (2021) 613–639.
[32] M.S. Arulampalam, S. Maskell, N. Gordon, T. Clapp, A tutorial on particle filters for online nonlinear/non-Gaussian Bayesian tracking, IEEE Trans. Signal Process. 50 (2002) 174–188.
[33] S. Torkamani, S. Roy, M.E. Barkey, E. Sazonov, S. Burkett, S. Kotru, A novel damage index for damage identification using guided waves with application in laminated composites, Smart Mater. Struct. 23 (2014), 095015.
[34] X.P. Qing, H.-L. Chan, S.J. Beard, A. Kumar, An active diagnostic system for structural health monitoring of rocket engines, J. Intell. Mater. Syst. Struct. 17 (2006) 619–628.

[35] J. Liu, M. West, Combined parameter and state estimation in simulation-based filtering, Sequential Monte Carlo methods in practice, in: A. Doucet, N. Freitas, N. Gordon (Eds.), Sequential Monte Carlo Methods in Practice, Springer New York, New York, NY, 2001, pp. 197–223.
[36] E.N. Chatzi, A.W. Smyth, The unscented Kalman filter and particle filter methods for nonlinear structural system identification with non-collocated heterogeneous sensing, Struct. Control Health Monit. 16 (2010) 99–123.
[37] A. Saxena, J. Celaya, E. Balaban, K. Goebel, B. Saha, S. Saha, M. Schwabacher, Metrics for evaluating performance of prognostic techniques, in: 2008 International Conference on Prognostics and Health Management, 2008, pp. 1–17.